Radiopharmaceutical properties of hydroxyapatite smaller than 50nm produced from eggshell and labeled with ^{99m}Tc and its biodistribution in rabbits

Aziz Gültekin[1*] MD,
Ayşe Uğur[2] MD,
Mine Sulak[3] MD,
Samiye Demirezen[1] MD,
Doğangün Yüksel[1] MD

1. Department of Nuclear Medicine, Medical Faculty, Pamukkale University, Denizli, Türkiye,
2. Department of Nuclear Medicine, Education and Research Hospital, Pamukkale University, Denizli, Türkiye,
3. Department of Mathematics and Science Education, Faculty of Education, Pamukkale University, Denizli, Türkiye.

Keywords: Nanohydroxyapatite
- Technetium-99m
- ^{99m}Tc-Nanohydroxyapatite
- Biodistribution
- Preclinical imaging

Corresponding author:
Aziz Gültekin, Assoc. Prof. Dr. Pamukkale University, Medical Faculty, Department of Nuclear Medicine, 20160, Denizli-Turkey
agultekin@pau.edu.tr

Received:
26 September 2024
Accepted revised:
15 January 2025

Abstract

Objective: Radiolabeling of nanoparticles has potential benefits for personalized treatments and theranostic applications, which have been on the agenda in recent years. Hydroxyapatite nanoparticles (HANP), which have a great similarity to bone tissue, stand out as a biocompatible nanoparticle. The different biodistribution properties of hydroxyapatite molecules in different nanosizes may create new opportunities for their use, especially in bone imaging and in the treatment of bone tumors. This study aims to investigate the labeling of hydroxyapatite molecules smaller than 50 nanometers obtained from eggshells with technetium-99m (^{99m}Tc) and the in vivo distribution of this molecule in rabbits. **Materials and Methods:** Characterization of nanohydroxyapatite particles obtained from eggshells was performed using scanning electron microscopy (SEM), energy dispersive X-ray (EDX), and X-ray diffraction (XRD). Radiolabeling of HANP smaller than 50nm with ^{99m}Tc radionuclide, stability of the labeled product, and biodistribution profile in rabbits were investigated. **Results:** The radiochemical purity of the ^{99m}Tc-HANP was obtained as 96%. The in vitro stability of ^{99m}Tc labeled HANP was examined for up to 12 hours and showed excellent in vitro stability for the first 4 hours in saline. Technetium-99m-HANP remained stable in vivo during the 6-hour imaging period. In quantitative analysis, ^{99m}Tc-HANP showed accumulation in bone tissue in the second hour. **Conclusion:** Technetium-99m-HANP nanoradiopharmaceuticals with sizes less than 50 nanometers (20-31nm) showed high uptake in bone tissue in rabbits. Therefore, HANP can be developed as imaging radiopharmaceuticals in bone tissue and bone cancers.

Hell J Nucl Med 2025; 28(1): 61-70 *Epub ahead of print: 7 April 2025* *Published online: 30 April 2025*

Introduction

With the rapid development of the theranostic definition, the diagnostic and therapeutic agents were loaded into the nanoparticles, and the definition of "nano theranostics" was born. Nanotheranostics applies nanomedicine strategies for advanced theranostics. Nanotheranostics provides a convenient window for monitoring the pharmacokinetics and pharmacodynamics of the drug injected into the body. With the help of nanostructures, an appropriate diagnosis and therapeutic intervention can be achieved by simultaneously targeting diseased cells and imaging the pathological regions after the systemic circulation of the drug [1].

The goal of theranostics is to optimize the efficacy and safety of treatment, as well as to facilitate the entire drug development process [2]. Nanomedicine has demonstrated excellent results in gene therapy, drug delivery, and clinical research [3]. Although there is no official definition of nanoparticles (NP), which are the basic elements of nanotechnology, they are called colloidal or polymeric particle systems with particle sizes ranging from 1 to 1000nm prepared with polymers of natural or synthetic nature (Figure 1) [4].

Different molecules have been investigated for the pharmacokinetics and biodistribution of NP [5, 6]. Nanoparticles design flexibility provides adjustable in vivo pharmacokinetics to improve delivery efficiency and reduce non-specific organ uptake by modifying size, charge, and surface modification. Nanoparticles with a diameter of about 100nm show prolonged blood circulation and relatively low mononuclear phagocyte system uptake [6, 7]. This dimension, which is between the macroscopic and molecular levels, also occupies a critical position at the cellular level. Therefore, nanosystems can be designed to have some superior properties. However, the residues of nanomaterials can have a detrimental effect on human health. The analysis of NP in different matrices should not be limited. Because the potential toxicity and behavior of NP can be affected by a wide variety of factors such as particle number, charge, size and size distribution, chemistry and reactivity, surface area, structure and shape, aggregation state, and elemental composition [8].

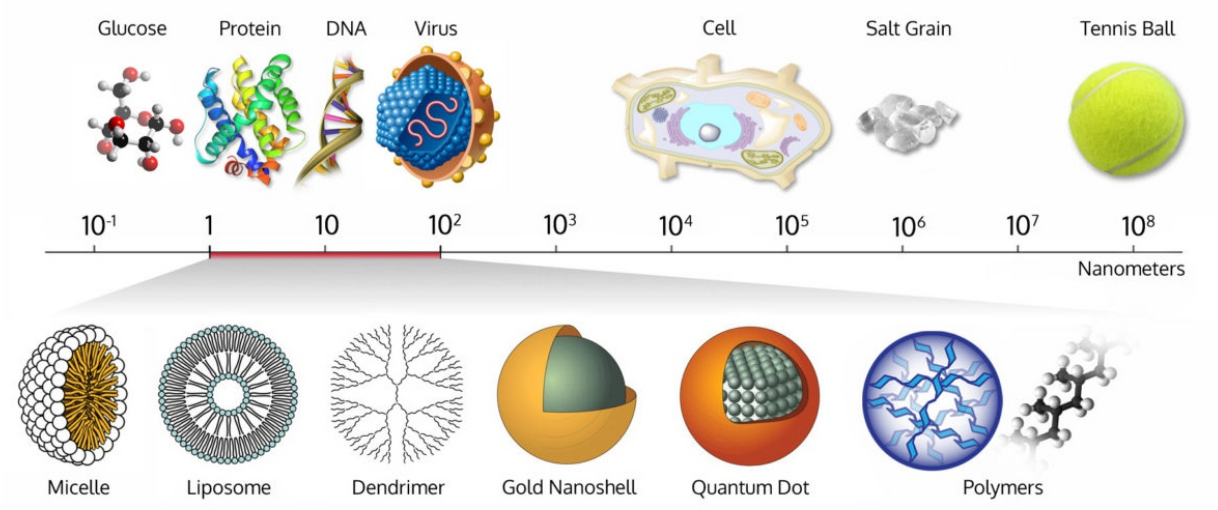

Figure 1. Nanoscale of nanoparticles and biomolecules*. *This figure was uploaded by Wich Research Lab. The content may be subject to copyright.

Different molecules have been investigated for the pharmacokinetics and biodistribution of NP [5, 6]. Nanoparticles design flexibility provides adjustable in vivo pharmacokinetics to improve delivery efficiency and reduce non-specific organ uptake by modifying size, charge, and surface modification. Nanoparticles with a diameter of about 100nm show prolonged blood circulation and relatively low mononuclear phagocyte system uptake [6, 7]. This dimension, which is between the macroscopic and molecular levels, also occupies a critical position at the cellular level. Therefore, nanosystems can be designed to have some superior properties. However, the residues of nanomaterials can have a detrimental effect on human health. The analysis of NP in different matrices should not be limited. Because the potential toxicity and behavior of NP can be affected by a wide variety of factors such as particle number, charge, size and size distribution, chemistry and reactivity, surface area, structure and shape, aggregation state, and elemental composition [8].

The use of nanosized particles in nuclear medicine provides numerous advantages in diagnosis and treatment. Radiopharmaceuticals obtained using nanomaterials provide an excellent platform for molecular imaging, diagnosis, and treatment of cancer [9]. When drug imaging agents are performed, drug delivery systems ensure safe, controlled and effective delivery of diagnostic imaging and/or therapeutic agents to the target organ or tissue. Due to the use of nanodrugs in drug delivery systems, various anatomical and biological structures such as the blood-brain barrier, bronchioles in the respiratory system, and tight junctions in the skin are overcome and the transported substance is delivered to the target tissue [10]. For example, nanosensors can measure a wide variety of biomarkers in a small sample volume [11, 12], and thanks to nanomedicine, drugs with low side effects can be administered in higher doses by active targeting of the blood vessels to the tumor site or receptor [12].

There are two main radiolabeling strategies for nanoparticles. The first is to make the NP structure itself radioactive, either at the surface or in the core. The other approach is to radioactively capture the charge encapsulated in the NP. Both approaches are commonly used for radiolabeling of NP. The technetium-99m (^{99m}Tc) radionuclide generator product is labeled with NP by the direct labeling method with a gamma energy of 140keV [13]. With the advent of multimodal nuclear medicine imaging, which combines both anatomical and physiological information, improved spatial resolution, increased detection sensitivity, and the availability of quantitative data have provided new opportunities for an accurate and precise diagnosis of cancer [14].

Calcium orthophosphate biomaterials have wide applications in medicine. Among them, synthetic hydroxyapatite [$Ca_{10}(PO_4)_6(OH)_2$] is promising for its use in medicine due to its biocompatibility and bioactivity. Hydroxyapatite nanoparticles (HANP) can be developed as nanoradiopharmaceuticals due to their physicochemical properties [15, 16]. Hydroxyapatite nanoparticles stands out as a biocompatible nanoparticle that shows great similarity to bone tissue [17]. Nanohydroxyapatite is an osteoconductive material that can stimulate bone matrix regeneration after surgical treatment of osteosarcoma [18]. Hydroxyapatite nanoparticles are easily synthesized by many different methods [19]. Another important feature of HANP is that, as a crystalline material, it is also possible to combine this material with other metals to give nanoparticles new properties, such as the combination with radioisotopes to provide theranostic properties [20]. Currently, inorganic nanoparticles such as hydroxyapatite, $BaSO_4$ NPs, Ag-NPs, $LaPO_4$ NPs, TiO_2 and superparamagnetic iron oxide NP are being examined as carrier molecules for diagnostic or therapeutic purposes in nuclear medicine. Hydroxyapatite has already been labeled with radionuclides such as ^{99m}Tc and fluorine-18 (^{18}F) for diagnostic purposes in nuclear medicine. Technetium-99m labeled HANP are shown as a potential candidate imaging agent for bone cancer imaging [21]. Due to the potential position of HANP in radionuclide diagnosis and treatment, more research is needed in this area that can be translated into the clinic.

This study consists of two parts. In the first part, we investigated the radiolabeling strategy of sub-50nm hydroxyapatite NP produced from eggshells with ^{99m}Tc radionuclide and the stability of the labeled NP. In the second part, we examine the biodistribution profile of this radiopharmaceutical in rabbits by scintigraphic imaging.

Materials and Methods

All reagents to be used for the synthesis and quality control of HANP and ^{99m}Tc-HANP radiopharmaceuticals were obtained from Sigma-Merck in high purity pharmaceutical grade. The Mon-Tek brand molybdenum-99 (^{99}Mo)/^{99m}Tc commercial generator available in the radiopharmacy laboratory of our department was used in the studies.

Nanohydroxyapatite synthesis

For hydroxyapatite nanoparticles synthesis, the eggshells were first separated from their membranes, then thoroughly washed with distilled water, and then the eggshells were dried. The eggshells were crushed and calcined at 900°C for 3 hours in a still air environment. Distilled water was added to the calcined egg shells to be used in the synthesis of the hydroxyapatite material and mixed for 60 minutes at room temperature in a magnetic stirrer [22]. The pH: 11 adjusted solution using NH_4OH was heated to 90°C and the reaction stirred for 2 hours. Cooled to room temperature, the solution was aged for 20 hours. The obtained nanoparticles were dried by filtration. The characterization of the obtained nanohydroxyapatites was performed using scanning electron microscopy (SEM), energy dispersive X-ray (EDX), and X-ray diffraction (XRD).

Nanohydroxyapatite radiolabelling with ^{99m}Tc

To provide optimal conditions for ^{99m}Tc maximum radiolabeling efficiency, different experiments were performed by varying reaction parameters such as ^{99m}Tc-HANP, HANP concentration, pH of the reaction mixture, and incubation time. In a reaction volume of 1mL, the amount of HANP used for radiolabeling ranged from 1 to 7mg and radiolabeling yields were determined in each case. The effect of change in pH on radiolabeling efficiency at room temperature was investigated at different pH values using the $NaHCO_3$ solution of the reaction mixture. The incubation time required to achieve maximum labeling efficiency was optimized by performing reactions for different times (0, 5, 10, 15, 20 minutes) at room temperature and determining the yields in each case.

For the labeling process, nanoparticles smaller than 50nm were obtained by passing them through a 0.45nm filter. Ready-to-mark solutions with ^{99m}Tc were obtained by mixing hydroxyapatite with stannous chloride ($SnCl_2$) at room temperature. One hundred μCi (approximately 300μL) of ^{99m}Tc eluate was used to label the optimal amount of HANP with ^{99m}Tc radionuclide.

Whatman paper No1 was used to characterize the labeled nanoparticles. Thin layer chromatography (TLC) was performed using 2μL of each labeled sample in acetone (Sigma-Aldrich) as the mobile phase. The radioactivity on the papers was confirmed in the Comecer brand dose calibrator. Radiolabeled product stability was determined by incubation for up to 12 hours while monitored by paper chromatography as detailed above.

The morphological structure of ^{99m}Tc-HANP, the synthesis product of the study, was microanalytically analyzed at the Advanced Technology Application and Research Center of our University. The 12-hour stability and particle degradation of ^{99m}Tc-HANP were investigated by SEM and EDX. For this purpose, selected samples for scanning electron microscopy analysis (Quorum Q150R-ES) were photographed at a magnification of 100.00X and EDX analysis was examined. The material was coated with 80% Au and 20% Pd. Au/Pd is used to ensure conductivity under the electron microscope (SEM). Image analyzes were performed on a secondary electron detector (SE2) on a Zeiss Supra 40Vp at a voltage of 30 KV.

Animal experiments procedure

This preclinical study was conducted after obtaining ethical approval from the Animal Experimentation Ethics Committee (24 May 2021; 2021/05). During the experiments, national and international directives were followed. The gender of the rabbits was not considered a factor in the experimental design. All rabbits were kept in separate cages with 12-hour day and night cycles at 25°C during treatments and fed ad libitum.

Six New Zealand rabbits (Oryctolagus cuniculus) weighing 2300-3000g were divided into 2 groups: ^{99m}Tc-HANP (n=3) and ^{99m}Tc (n=3). All rabbits were injected intramuscularly with 35mg/kg ketasol (Ketasol 10mL, Richterpharma, Austria) and xylazine 5mg/kg (Rompun 25mL, Bayer, USA) to induce general anesthesia. To determine the biodistribution of ^{99m}Tc-HANP in rabbits, three rabbits were injected intravenously with 37MBq/kg of ^{99m}Tc-HANP through the ear vein after anesthesia. The imaging was performed with a dual-detector hybrid gamma camera coupled to flat panel computed tomography (CT) with a low-dose X-ray tube (2.5mA, 120kVp; Philips Brightview XBT) in the same portal (Cleveland, Ohio, USA). Whole body static images were obtained at 10, 20, 30, 40, 50, 60, 120, 240, and 360 minutes from rabbits lying in prone position under the Gamma Camera. For comparison, 37MBq/kg of ^{99m}Tc was injected into the ear vein of the other three rabbits after anesthesia and static images of the whole body were obtained at 10, 20, 30, 40, 50, 60, 120, 240, and 360 minutes. The regions of interest were drawn in the regions of the heart, lung, liver, spleen, kidney, bone, muscle, and thyroid of the images obtained from the ^{99m}Tc- HANP rabbits and the ^{99m}Tc group rabbits. Counts taken between 10 minutes and 6 hours for each organ were recorded in count/pixel. Time (minute)/radioactivity (counts/pixels) curves were created for all organs and the biological distribution of ^{99m}Tc-HANP and ^{99m}Tc was examined for 6 hours. The biodistributions of ^{99m}Tc-HANP and ^{99m}Tc in rabbits were compared with each other.

Statistical analysis

Data were analyzed with SPSS 24.0 software package (IBM, Armonk, NY, USA). Continuous variables are given as mean± standard deviation and categorical variables are given as frequency and percentage.

Results

Hydroxyapatite nanoparticle synthesis

The morphology and elemental analyzes of the obtained hydroxyapatite nanoparticles were confirmed by SEM, EDX (Scanning Electron Microscope/Energy Dispersion XRD) with FEI Quanta 400F device at our University Advanced Technology Application and Research Center (Figure 2).

After the samples were coated with 3nm thick gold-palladium, images of the supports and immobilized supports prepared with field emission electron gun were taken at room temperature under high vacuum conditions (Figure 3).

XRD patterns of synthesized nanoparticles were obtained using 80 XRD diffractometry (XRD) APD 2000 PRO diffractometer instrument (GNR, Novara, Italy) in the range of 5° to 90° 2θ with Cu Kα beam (λ=1.54 Å) (Figure 4). The Joint Committee on Powder Diffraction Standards (JCPDS) XRD data analysis card was compared with the obtained XRD spectra. The size of the obtained hydroxyapatite nanoparticels were calculated according to the Debye-Scherer equation [23].
Debye Scherrer equation:

$$D = \frac{k\lambda}{\beta Cos\,\theta}$$

D; Average crystallite size, K; a constant equal to 0.94, λ; to the wavelength of X-rays radiation (0.154nm), β; The width of the apex of the crown slit (in radians) and 2θ; It corresponds to the Bragg angle (degrees).

Labeling of nano-hydroxyapatite particles with ^{99m}Tc

The effect of the change in the amount of HANP used in radiolabeling on the ^{99m}Tc-labeled HANP yield is shown in Figure 5a. A radiolabeling efficiency of 75%±1 was achieved with 1mg of HANP in a 1mL reaction volume, while it increased to 96%±0.5 when 5mg of HANP were used. As a result, 5mg/mL was accepted as the optimal ligand concentration for further studies. Other parameters were performed at pH~5 at room temperature. Below pH 4 and after pH 6 the radiolabeling efficiency was found to be poor (Figure 5b). When the radiolabeling efficiency was determined at different incubation times during the reaction, it was observed that the yield gradually increased with the reaction time when the reactants were left to incubate for 15 minutes at room temperature.

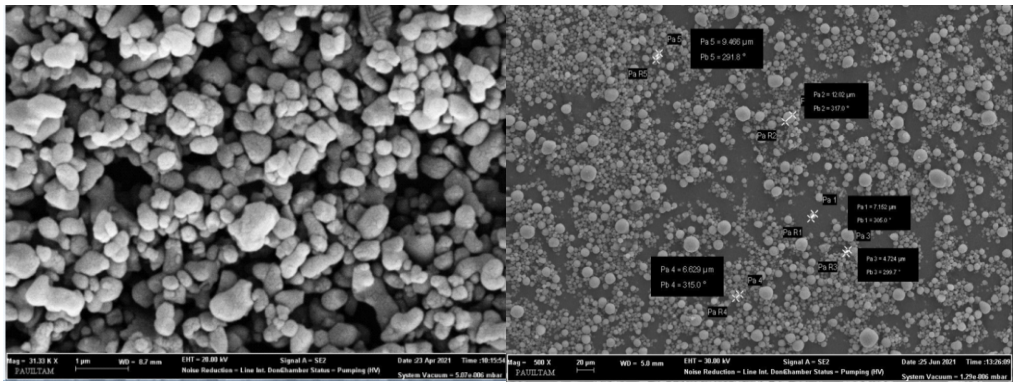

Figure 2. SEM analysis images of HANP (SEM images; 200nm, Mag x25000, EHT 30.00KV)

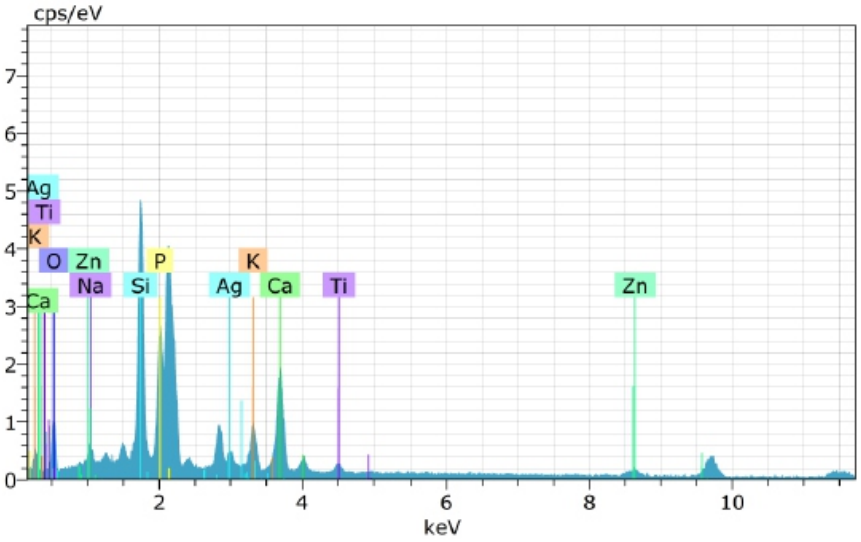

Figure 3. EDX analysis for hydroxyapatite nanoparticles from eggshell.

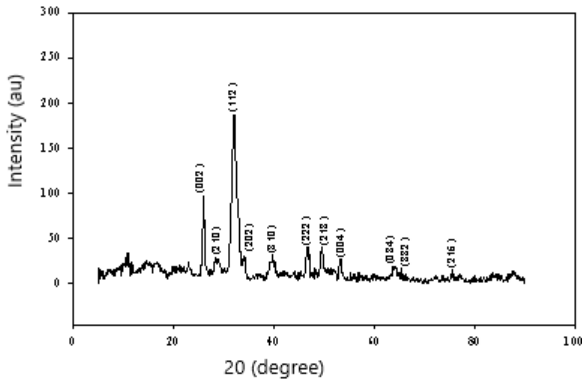

Figure 4. X-rays diffractogram/diffraction patterns of HANP.

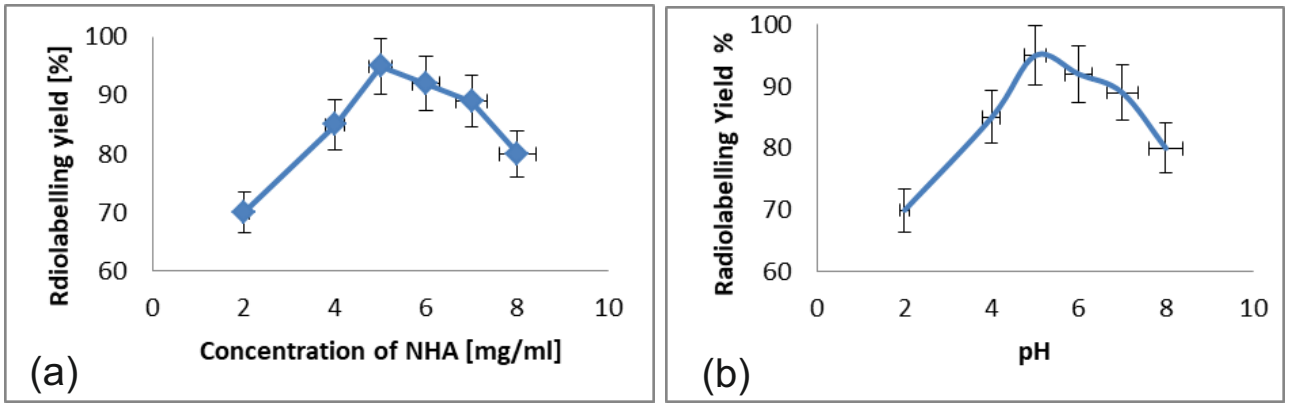

Figure 5. a) Effect of the change in the amount of HANP on radiolabeling efficiency, b) Effect of pH on radiolabeling efficiency.

In vitro, stability studies were performed using the TLC method. Hydroxyapatite nanoparticles labeled with ^{99m}Tc showed excellent in vitro stability in saline for up to 12h. In the TLC method, the free TcO_4 in the strips leaves the labeled complex at the bottom of the strip and migrates towards the front. The radiolabeled complex remains at the point of application. The excess of stannous chloride used for the reduction of pertechnetate causes the formation of undesirable radiocolloids. Therefore, the percentage of radiocolloid was determined using pyridine: acetic acid: water (3:5: 1.5). The free pertechnate and the labeled complex moved to the front of the strip, while the colloids remained at the bottom of the strip. The net amount of ^{99m}Tc-HANP was calculated by subtracting the activity fraction migrating in acetone from the mixture of pyridine: acetic acid: water. The radiochemical purity of ^{99m}Tc-HANP used in animal studies was calculated as 96%.

The binding of ^{99m}Tc-labeled HANP was examined for structural degradation for 12 hours (Figure 6). SEM analyzes showed that ^{99m}Tc-HANP nanoradiopharmaceutical remained in the original size range at first labeling but underwent structural degradation at 12 hours.

Biodistribution of ^{99m}Tc-HANP in rabbits

When the biodistribution of ^{99m}Tc and ^{99m}Tc-HANP in rabbits was visually evaluated, uptake was not observed in the thyroid gland and gastrointestinal tract in the ^{99m}Tc-HANP images. In ^{99m}Tc biodistribution images, uptake of activity in the thyroid gland and gastrointestinal tract increased as expected.

In ^{99m}Tc-HANP images, increased activity uptake was detected in the liver, spleen, kidney, and bone tissue compared to ^{99m}Tc physiological distribution images (Figure 7).

In quantitative data; When the time/radioactivity curve is examined, it is observed that ^{99m}Tc and ^{99m}Tc-HANP have similar biodistribution curves in bone tissue until the second hour. However, after the second hour, ^{99m}Tc-HANP shows stable uptake in bone tissue compared to ^{99m}Tc. After the second hour, the uptake of ^{99m}Tc in bone tissue decreased (Figure 8).

When the time/radioactivity curve generated by the thyroid gland was examined, ^{99m}Tc uptake in the thyroid gland increased until the 50th minute and then slowly washed out. No ^{99m}Tc-HANP uptake was observed in thyroid tissue for 6 hours (Figure 7). It created a blood-pool-like washout curve (Figure 9).

The relative biodistribution of ^{99m}Tc-HANP in the rabbit body according to the organs is shown in the graph (Figure 10).

In heart and lung biodistribution images, ^{99m}Tc-HANP uptake in heart and lung was observed to be lower than ^{99m}Tc until the second hour. They then draw a similar washout curve.

No accumulation of ^{99m}Tc-HANP was observed in the intestines. This shows that labeled HANPs are not excreted through the liver/bile (Figure 7).

Table 1. *Stability analysis with HANP with ^{99m}Tc.*

	Time in hours					
(%)	**0**	**1**	**2**	**4**	**8**	**12**
Labeling	96,0					
Analysis-1	96,0	95,0	95,0	94,0	90,0	50,0
Analysis-2	96,0	95,5	94,0	94,0	89,5	51,0
Analysis-3	95,5	95,5	94,5	93,0	90,0	45,0
Average	95,7	95,3	94,5	93,7	89,7	48,5

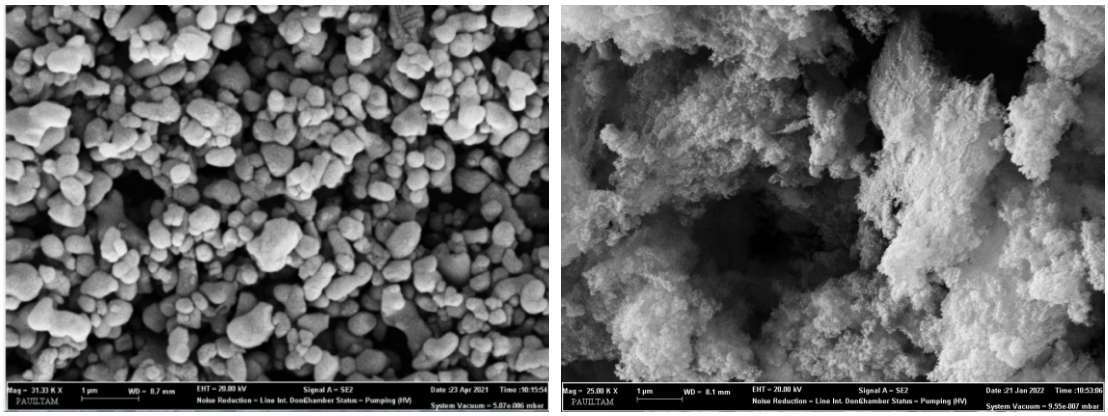

Figure 6. a) SEM analysis images of ^{99m}Tc-HANP (SEM images; 200nm, Mag x25000, EHT 20.00KV), b) 12th hour stability image (SEM images; 200nm, Mag x40000, EHT 20.00KV)

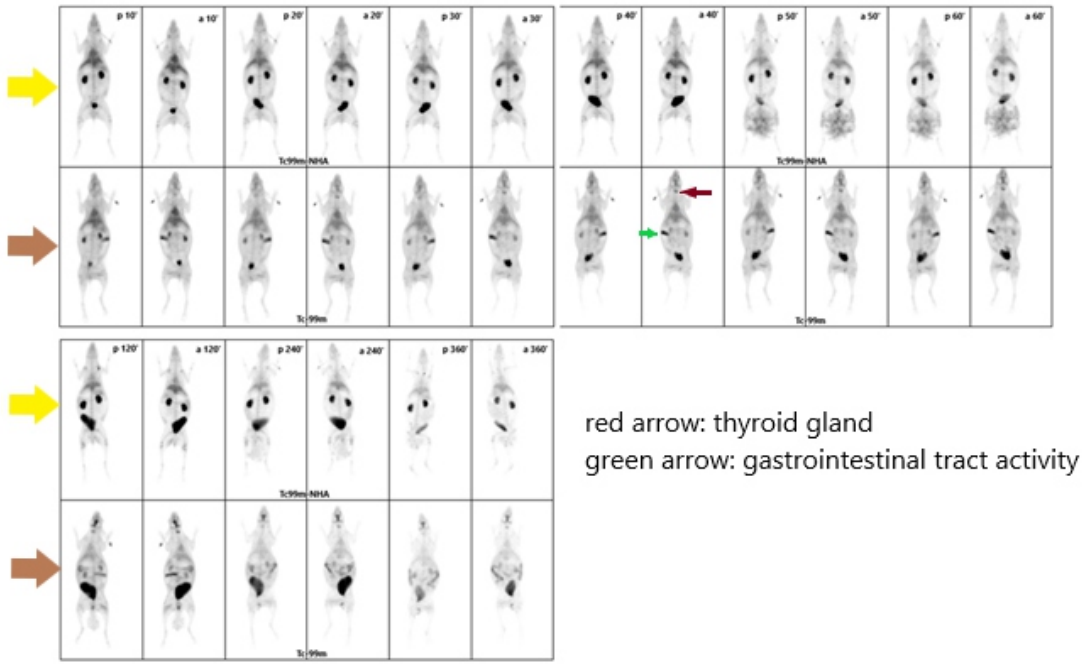

Figure 7. Six hours of biodistribution of ^{99m}Tc-HANP and ^{99m}Tc in rabbits. The first row shows ^{99mT}c-HANP (yellow arrows) and the second row ^{99m}Tc (brown arrows) biodistribution images.

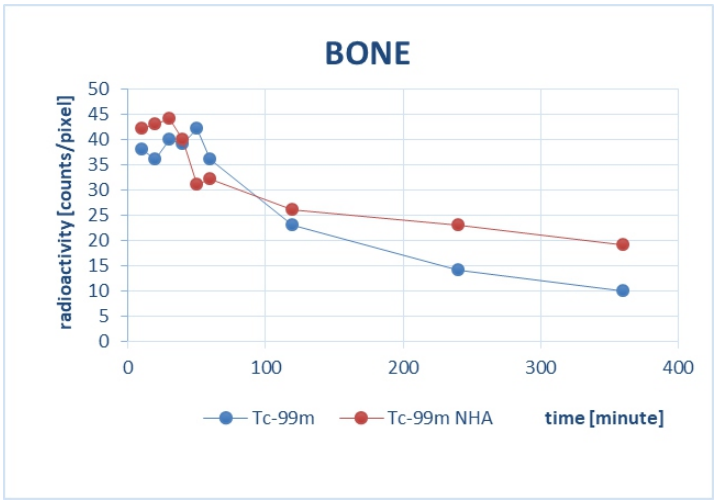

Figure 8. Time/radioactivity graph for ^{99m}Tc and ^{99m}Tc-HANP of the bone.

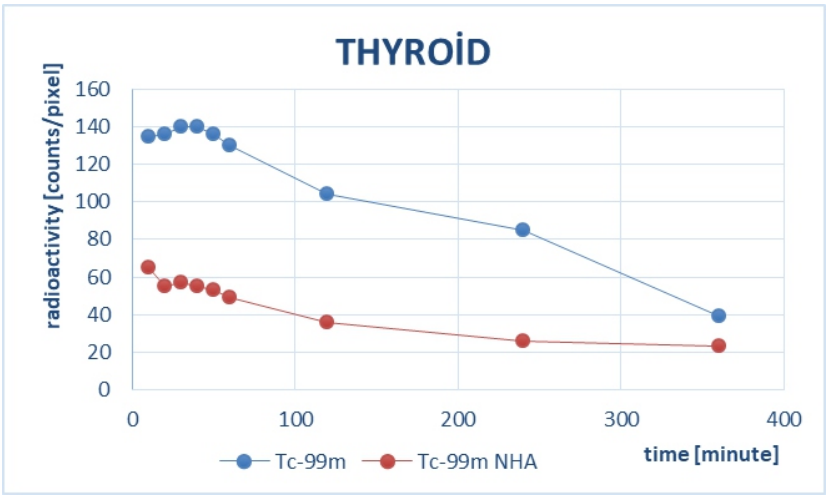

Figure 9. Time/radioactivity graph for ^{99m}Tc and ^{99m}Tc-HANP of the thyroid gland.

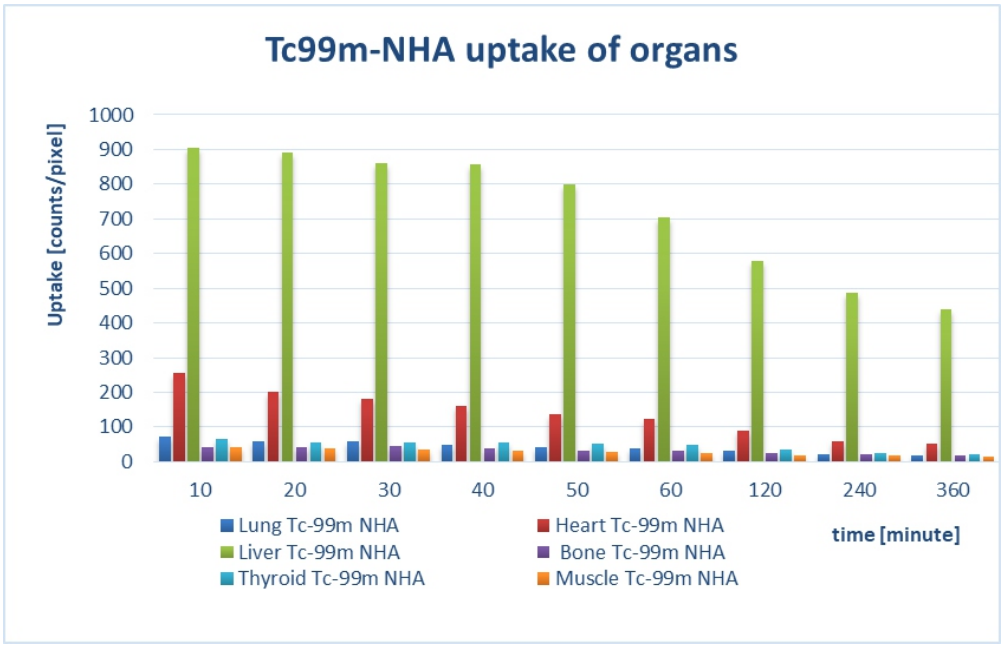

Figure 10. Relative uptake rates of ^{99m}Tc-HANP in the lung, heart, liver, bone, thyroid and muscle.

Discussion

Hydroxyapatite (HA) is the natural mineral component of the bone matrix. Hydroxyapatite is biocompatible and biodegradable. It can be easily labeled with radionuclides. As a biological agent, its half-life is longer than that of the radionuclides studied. Hydroxyapatite particles are converted to Ca^{+2} and PO_4^{-3} ions by natural metabolic processes and are eliminated within 6 weeks, ensuring biocompatibility [24-26]. Hydroxyapatite is the main inorganic component of dental enamel and biological bone and shows excellent biocompatibility and bioactivity. It is used as a biomedical material in orthopedics and dental implants. Hydroxyapatite nanoparticles have highly active surfaces and are used as carriers in drug delivery systems [22]. Interestingly, HANP can inhibit the growth of some cancer cells [27, 28]. In an experimental study, the healing of a bone defect treated with HANP was visualized scintigraphically with ^{99m}Tc-bisphosphonates [29]. We synthesized HANP from the egg shell. This method is both cheap and easy. Previously, Siddharthan and his colleagues synthesized Hydroxyapatite nanoparticles from eggshells using a similar method [30]. The surface of HANP was examined morphologically from the SEM image of nanosized hydroxyapatite obtained from eggshells in a basic medium. As a result of the examination, it was determined that the particles were dispersed on a nanoscale, spherical, and homogeneous manner and the particle sizes were 20-31nm on average. Our results were consistent with those of Sopyan et al. (2009) [31]. The size, shape, and surface properties of HANPs are important for biodistribution. Agents administered parenterally below the glomerular filtration limit (<5nm in diameter) are rapidly excreted by the kidneys. Larger NP remain in circulation longer. It often accumulates in the liver and spleen, whereas micrometer-sized particles become stuck in capillary beds and in the pulmonary vasculature. The surfaces of nanoparticles are often modified with a polysaccharide or polymer; coatings increase the circulation time of the particle and provide greater uptake in regions of interest. Highly charged and hydrophobic particles increase the diameter of the nanoparticle and enable it to be recognized by the reticuloendothelial system. Particles below 100nm in diameter can persist in circulation for longer periods, allowing nonspecific imaging of disease sites through enhanced permeability and retention effect (EPR) [32].

The EDX spectrum of the hydroxyapatite nanoparticles is shown in Figure 2. The presence of calcium, phosphate, and oxygen elements in the structure of the prepared HANP is clearly seen in the figure. The findings obtained from the EDX analysis are also in agreement with the results of the SEM and XRD analysis.

The XRD (powder) method was used to determine the crystal formation of the synthesized nanoparticular hydroxyapatite. Figure 4 shows the nanohydroxyapatite X-rays model. According to the COD library, it was determined that the hydroxyapatite nanoparticles obtained from the eggshell were hexagonal in structure and the lattice parameters were a=9.416, c=6.874 (COD card number: 96-900-12 34). The average particle size calculated according to the Debye-Scherrer formula is approximately 16.45nm [23].

In the development of a radiopharmaceutical, all necessary parameters such as radiochemical purity, stability, and reproducibility should be examined, as well as the ability to obtain it with high yield. In our study, ^{99m}Tc-labeled high-efficiency HANP were obtained, and it was determined that radiopharmaceuticals could be easily applied by a radiopharmacist in nuclear medicine laboratories, and radiation safety was provided. In vivo stability of radiolabeled particles is important in visualizing the uptake of the labeled radiopharmaceutical in relevant tissue. Since the separation of the nanoparticles from the radionuclide will shorten its life in the biological system, its in vitro stability should be at least as long as the physical half-life of the radionuclide. In our study, we obtained nanoradiopharmaceuticals with a 96% binding percentage to HANP produced from eggshell and ^{99m}Tc radionuclide. Albernaz et al. (2014) [33] developed radiolabeled nanoparticles with ^{99m}Tc and studied bone cancer imaging. Their results indicate that labeling of nanoparticles is possible because of the hydroxyapatite and its physicochemical properties. They stated that it is possible to develop nanoradiopharmaceuticals for bone. In their study, they made labeling in radiochemical yield compatible with our study. Our in vitro stability results showed that ^{99m}Tc-HANP can be used clinically in short-term [4-hour] stability studies, but the nanoparticle undergoes structural degradation at equilibrium with a half-life of ^{99m}Tc at 12 hours. This result is consistent with the low percentage of binding at 12 hours in the experimental results of the labeling activity.

In our study, we visualized the biodistribution of ^{99m}Tc-HANP by scintigraphy. We injected only ^{99m}Tc into rabbits in the control group. By comparing ^{99m}Tc-HANP and ^{99m}Tc images, we evaluated the pharmacokinetics of ^{99m}Tc-HANP as more reliable. We also examined the in vivo stability of ^{99m}Tc-HANP by observing thyroid and stomach uptake in the ^{99m}Tc-HANP group at a 6-hour follow-up.

The radiopharmaceutical ^{99m}Tc-HANP, obtained by labeling HANPs smaller than 50 nanometers with ^{99m}Tc, had high uptake in the liver and spleen. An increase in ^{99m}Tc-HANP uptake in bones was observed at the 120th minute.

The only study similar to ours is the Albernaz et al. (2014) [33] in mice that showed a 5-minute distribution. In imaging targeting bone tissue, we think that 5 minutes of imaging time is too short to evaluate biodistribution. Therefore, our 6-hour biodistribution study is more valuable in terms of measuring the in vivo distribution and stability of the radiopharmaceutical. Monitoring high metabolism in the liver and spleen may decrease uptake in the target tissue. High liver uptake of ^{99m}Tc-HANP may cause problems in imaging and treatment. Therefore, by labeling different nanosizes of hydroxyapatite with radionuclides, optimal bone/liver or bone/background uptake ratios can be discovered. Additionally, using different administration methods, such as local administration of the radiopharmaceutical instead of parenteral administration, can prevent nanoradiopharmaceuticals from being metabolized in the liver or liver toxicity when used in treatment. The absence of uptake in the thyroid gland and gastrointestinal tract in ^{99m}Tc-HANP biodistribution images in six hours of imaging indicates that the radiopharmaceutical maintains its stability in vivo in 6 hours.

When the diagnostic and treatment potentials of nanohydroxy apatite for bone cancer are reviewed, it can be com-

pared with a Swiss army knife. In studies conducted on many cell lines and animal models, HANP have natural antitumor effects. Reduction of tumor cell adhesion, induction of apoptosis and cell cycle arrest, and downregulation of telomerase activity are known antitumor mechanisms [34]. Nanohydroxy apatite is used as a good filling material and inorganic skeleton to repair operated bone cancers. After bone resection, residual tumor tissue must be treated with chemotherapy or radiation therapy. These treatments are highly toxic treatments. To reduce this toxicity, HANP can be designed as antitumor drug delivery systems. Thus, the effectiveness of the drug is increased and its toxicity is reduced. Hydroxyapatite nanoparticles have promising results in this field, due to their simultaneous antitumor, osteogenesis, and sustained drug release effects [35]. Photothermal therapy (PTT) and magnetic hyperthermia (MFH) are new treatment methods applied with the help of HANP in bone cancers [36, 37].

In the theranostic approach, HANP can be labeled with imaging agents (^{99m}Tc, ^{18}F) and therapeutic radionuclides that emit beta and alpha radiation (^{177}Lu, ^{166}Ho, ^{89}Sr, ^{32}P, ^{223}Ra) [26, 38].

One of the most important advantages of HANP is that they can be produced at the desired nanoscale. While smaller molecules are more useful for systemic treatments, larger HANP molecules that cannot pass through capillaries and reach the lymphatic system can be used in treatments such as radiation synovectomy, such as transarterial radioembolization (TARE).

The easy and inexpensive production of HANP is one of its most important advantages. In our study, eggshell was used as a raw material. The eggshell is an easily accessible and inexpensive material.

Hydroxyapatite nanoparticles are a natural substance already found in bone structure and do not cause immune reactions. It is easily metabolized and excreted. It does not leave waste in the organism.

Hydroxyapatite nanoparticles have great potential, especially in cancer diagnosis and treatment. Today, very few preclinical studies have been translated into the clinic. However, we predict that clinical applications related to HANP will increase rapidly.

In conclusion, ^{99m}Tc-HANP nanoradiopharmaceuticals with dimensions less than 50 nanometers (20-31nm) showed higher uptake in bone tissue in rabbits from the 120th minute. Therefore, HANP can be developed as an imaging agent in bone tissue and bone cancers. Due to its 6-hour in vivo stability, it provides sufficient conditions for imaging. The low in vitro stability of ^{99m}Tc-HANP at 12 hours and their high uptake into the liver in in vivo imaging constitute a disadvantage in terms of being a potential treatment agent. This situation can be resolved by producing HANP in different sizes and different modifications. Producing HANP from eggshells is advantageous in terms of cost. Additionally, it can be easily labeled with radionuclides, which makes it have a theranostic potential. When produced in different molecular sizes and by adding different surface features, HANP can open new horizons in the diagnosis and treatment of bone cancer and some other cancers.

The authors declare that they have no conflicts of interest

Acknowledgement

This study was supported by the Pamukkale University Scientic Research Coordination Unit under project number 2021HZDP018.

Ethics Committee Approval

The Law on the Protection and Welfare of Animals applies to experiments with animals (PAUHADYEK 24 May 2021; 2021/05) in Turkey.

Bibliography

1. Kalash RS, Lakshmanan VK, Cho CS, Park IK. Theranostics. In: M. Ebara [Ed.], Biomaterials Nanoarchitectonics, 2016, p.197-215. 1st Edition. Elsevier Inc.: William Andrew.
2. Aulić S, Bolognesi ML, Legname G. Small-molecule theranostic probes: a promising future in neurodegenerative diseases. *Int J Cell Biol* 2013; 2013: 150952.
3. National Cancer Institute Web site. [2004]. "Cancer and Nanotechnology". Retrieved Jan 25; 2024. from https:// https://www.cancer.gov/nano/cancer-nanotechnology
4. Borm PJ, Robbins D, Haubold S et al. The potential risks of nanomaterials: a review carried out for ECETOC. *Part Fibre Toxicol* 2006; 3: 11.
5. Khlebtsov N, Dykman L. Biodistribution and toxicity of engineered gold nanoparticles: a review of in vitro and in vivo studies. *Chem Soc Rev* 2011; 40(3): 1647-71.
6. Li SD, Huang L. Pharmacokinetics and biodistribution of nanoparticles. *Mol Pharm* 2008; 5(4): 496-504.
7. Dağlıoğlu Y, Yılmaz HÖ. Nanopartikül Karakterizasyon Yöntemleri ve Ekotoksisite Deneylerindeki Önemi. *Marmara Fen Bilimleri Dergisi* 2018; 1: 1-17
8. Pal S, Tak YK, Song JM. Does the antibacterial activity of silver nanoparticles depend on the shape of the nanoparticle? A study of the Gram-negative bacterium Escherichia coli. *Appl Environ Microbiol* 2007; 73(6): 1712-20.
9. Chapman S, Dobrovolskaia M, Farahani K et al. Nanoparticles for cancer imaging: The good, the bad, and the promise. *Nano Today* 2013; 8(5): 454-60.
10. Wickham TJ. Ligand-directed targeting of genes to the site of disease. *Nat Med* 2003; 9(1): 135-9.
11. Swierczewska M, Liu G, Lee S, Chen X. High-sensitivity nanosensors for biomarker detection. *Chem Soc Rev* 2012; 41(7): 2641-55.
12. Chikkaveeraiah BV, Bhirde AA, Morgan NY et al. Electrochemical immunosensors for detection of cancer protein biomarkers. *ACS Nano* 2012; 6(8): 6546-61.
13. Kagadis GC, Loudos G, Katsanos K et al. In vivo small animal imaging: current status and future prospects. *Med Phys* 2010; 37(12): 6421-42.
14. Ge J, Zhang Q, Zeng J et al. Radiolabeling nanomaterials for multimodality imaging: New insights into nuclear medicine and cancer diagnosis. *Biomaterials* 2020; 228: 119553.
15. Chakraborty S, Vimalnath KV, Rajeswari A et al. Preparation, evaluation, and first clinical use of ^{177}Lu-labeled hydroxyapatite [HA] particles in the treatment of rheumatoid arthritis: utility of cold kits for convenient dose formulation at hospital radiopharmacy. *J Labelled Comp Radiopharm* 2014; 57(7): 453-62.
16. Orlova MA, Nikolaev AL, Trofimova TP et al. Hydroxyapatite and porphyrin-fullerene nanoparticles for diagnostic and therapeutic delivery of paramagnetic ions and radionuclides. *Bulletin of RSMU* 2018; 6: 86-93.
17. Wijesinghe W.P.S.L, Mantilaka M.M.M.G.P.G, Premalal E.V.A et al. Facile synthesis of both needle-like and spherical hydroxyapatite nanoparticles: Effect of synthetic temperature and calcination on morphology, crystallite size and crystallinity. *Mater Sci Eng C* 2014; 42: 83-90.
18. Santos C, Gomes P, Duarte J.A et al. Development of hydroxyapatite nanoparticles loaded with folic acid to induce osteoblastic differentiation. *Int J Pharm* 2017; 516: 185-95.
19. Ganachari Dr. Sharanabasava, Bevinakatti Anjali, Yaradoddi Jayachandra et al. Rapid synthesis, characterization and studies of hydroxyapatite nanoparticles. *Adv Mater Sci Res* 2016; 1(1): 9-13.

20. Cipreste M.F, Peres A.M, Cotta A.A.C et al. Synthesis and characterization of 159 Gd-doped hydroxyapatite nanorods for bioapplications as theranostic systems. *Mater Chem Phys* 2016; 181: 301-11.
21. Suchánková P, Kukleva E, Nykl E et al. Hydroxyapatite and Titanium Dioxide Nanoparticles: Radiolabelling and In Vitro Stability of Prospective Theranostic Nanocarriers for ^{223}Ra and ^{99m}Tc. *Nanomaterials [Basel]* 2020; 10(9): 1632.
22. Yan-Zhong Z, Yan-Yan H, Jun Z et al. Characteristics of functionalized nano-hydroxyapatite and internalization by human epithelial cell. *Nanoscale Res Lett* 2011; 6(1): 600.
23. Sumadevi K, Krishnamurthy G, Walmik P et al. Photocatalytic degradation of eriochrome black-T and evan's blue dyes under the visible light using PVA capped and uncapped Ag doped Zns nanoparticles. *Emergent Mater* 2021; 4: 447-56.
24. Das T, Banerjee S. Theranostic Applications of Lutetium-177 in Radionuclide Therapy. *Curr Radiopharm* 2016; 9(1): 94-101.
25. Zhu J, Wang H, Liao L et al. Small mesoporous silica nanoparticles as carriers for enhanced photodynamic therapy. *Chem Asian J* 2011; 6(9): 2332-8.
26. Unni PR, Chaudhari PR, Venkatesh M et al. Preparation and bioevaluation of ^{166}Ho labelled hydroxyapatite [HA] particles for radiosynovectomy. *Nucl Med Biol* 2002; 29(2): 199-209.
27. Liu ZS, Tang SL, Ai ZL. Effects of hydroxyapatite nanoparticles on proliferation and apoptosis of human hepatoma BEL-7402 cells. *World J Gastroenterol* 2003; 9(9): 1968-71.
28. Xu K, Wang Y, Xie Y et al. Anti-melanoma effect and action mechanism of a novel chitosan-based composite hydrogel containing hydroxyapatite nanoparticles. *Regen Biomater* 2022; 9: rbac050.
29. Zhu W, Wang D, Zhang X et al. An experimental study on the application of radionuclide imaging in repair of the bone defect. *Bosn J Basic Med Sci* 2011; 11(3): 163-8.
30. Siddharthan A, Kumar TS, Seshadri SK. Synthesis and characterization of nanocrystalline apatites from eggshells at different Ca/P ratios. *Biomed Mater* 2009; 4(4): 045010.
31. Sopyan I, Natasha AN. Preparation of nanostructured manganese-doped biphasic calcium phosphate powders via sol-gel method. *Ionics* 2009; 15: 735-41.
32. Abou DS, Pickett JE, Thorek DL. Nuclear molecular imaging with nanoparticles: radiochemistry, applications and translation. *Br J Radiol* 2015; 88(1054): 20150185.
33. Albernaz Mde S, Ospina CA, Rossi AM, Santos-Oliveira R. Radiolabelled nanohydroxyapatite with ^{99m}Tc: perspectives to nanoradiopharmaceuticals construction. *Artif Cells Nanomed Biotechnol* 2014; 42(2): 88-91.
34. Zhang Q, Qiang L, Liu Y et al. Biomaterial-assisted tumor therapy: A brief review of hydroxyapatite nanoparticles and its composites used in bone tumors therapy. *Front Bioeng Biotechnol* 2023; 11: 1167474.
35. Liu Y, Qiao Z, Gao J et al. Hydroxyapatite-Bovine Serum Albumin-Paclitaxel Nanoparticles for Locoregional Treatment of Osteosarcoma. *Adv Healthc Mater* 2021; 10(2): e2000573.
36. Xin Zhang, Jun Ma. Photothermal effect of 3D printed hydroxyapatite composite scaffolds incorporated with graphene nanoplatelets. *Ceramics International* 2021; 47: 6336-40.
37. Zhu Y, Yang Q, Yang M et al. Protein corona of magnetic hydroxyapatite scaffold improves cell proliferation via activation ofmitogen-activated protein kinase signaling pathway. *ACS Nano* 2017; 11(4): 3690-704.
38. Chakraborty S, Das T, Sarma HD et al. Preparation and preliminary studies on ^{177}Lu-labeled hydroxyapatite particles for possible use in the therapy of liver cancer. *Nucl Med Biol* 2008; 35(5): 589-97.